Macromolecules
NOTE

Macromolecules **2010**, *43*, 6237–6240
DOI: 10.1021/ma100998k

Polymeric Crystallization under Nanoscale 2D Spatial Confinement

Tsai-Ming Chung,[†] Tzu-Chung Wang,[†] Rong-Ming Ho,*[,†] Ya-Sen Sun,*[,‡] and Bao-Tsan Ko[§]

[†]*Department of Chemical Engineering, National Tsing Hua University, Hsinchu 30013, Taiwan,*
[‡]*Department of Chemical and Materials Engineering, National Central University, Taoyuan 32001, Taiwan, and* [§]*Department of Chemistry, Chung Yuan Christian University, Chungli 32023, Taiwan*

Received May 4, 2010; Revised Manuscript Received May 27, 2010

Introduction

Recently, much effort is devoted to precisely control over the spatial and anisotropic order of crystalline textures for semicrystalline polymers in a nanoscale confined space, by which they offer diverse and versatile benefits as potential applications in nanotechnologies.[1] Different approaches have been carried out in order to explore the effect of confinement on polymeric crystallization.[2−16] The self-assembled microdomains of semicrystalline block copolymers (BCP) are widely used to tailor over the spatial and anisotropic order of crystalline textures for crystallizable blocks as a model to understand the behavior of polymeric crystallization under nanoscale confinement.[2−11] In the cases of BCPs with hard confinement (i.e., vitrified confined condition) and strong segregation strength (i.e., significantly incompatible constituted blocks), crystallization kinetics can be tailored by not only altering circumstances with one-dimensional (lamellae-forming microdomain), two-dimensional (cylinder-forming microdomain), and three-dimensional (sphere-forming microdomain) confinement but also by changing the confined size due to the variation on frustrating polymeric crystallization.[2−11] Reducing in confined size leads to a distinct transformation of isothermal crystallization kinetics, from heterogeneous to homogeneous nucleation, when the confined size becomes smaller than a critical dimension (i.e., heterogeneously crystallized lamellar thickness of homopolymers in most of the crystallization temperature region) to experience effective confinement. The change in crystallization kinetics led to an abrupt shift in crystallization to the low-temperature region and resulted in the generation of discrete crystalline granules through homogeneous nucleation, namely a single nucleus within one granule.[17] Also, altering the confined size has a significant effect on crystal growth (i.e., crystalline orientation) of crystallizable materials between vitrified layers; the orientation of crystals may adopt the perpendicular type once confined space approaches submicrometer scale.[7,18]

The effects of altering confine size on polymer crystallization have been widely studied in lamellae-forming BCPs;[7,17,18] however, such effects between crystal nucleation and growth and confined size are yet to be clarified in cylinder-forming block copolymers. In this extended note, we aimed to examine how crystal nucleation and growth may be related to the effects of altered size of cylindrical spatial confinement (i.e., 2D confinement). Similar to the results under 1D confinement, not only does reducing confinement space to an effective size make it possible to nucleate homogeneously as governing an overall crystallization process, but also reducing confinement space causes the crystal growth of PCL blocks changing from preferred crystalline orientation to random orientation. As a result, this system could serve as a model to analyze the impact of confined size on polymeric crystallization under 2D confinement.

Experiments

Materials. Semicrystalline P4VP−PCL BCPs were synthesized via living ring-opening polymerization (ROP) and atom-transfer radical polymerization (ATRP) in sequence.[19] First, we prepared a benzyl ester end-functionalized poly(ε-caprolactone), PCL−OH, resulting from the ROP of ε-caprolactone monomers. A chloride-terminated PCL was then prepared as a macroinitiator that served for the controlled polymerization of 4-vinylpyridine. Detailed synthetic routes were described in our previous paper.[17] The P4VP−PCL BCPs were briefly designated as VP/CL m/n in which m and n represent the degree of polymerization of each constituted block. The characterization of the resultant BCPs is tabulated in Table 1.

Sample Preparation. Bulk sample of BCPs were prepared by solution casting from dichloromethane (CH_2Cl_2) solution (10 wt % of P4VP−PCL) at room temperature. To examine the grown crystal orientation under confinement, the cylinder-forming samples were subjected to a large-amplitude oscillating shear at 190 °C to achieve a uniform, parallel alignment of the cylindrical microdomains by removing defects and grain boundaries. The shear apparatus was aerated with nitrogen gas to prevent thermal degradation. The shear geometry was described as follows: the shear direction is along the x direction, and the shear gradient is along the z direction. The shear frequency was 0.5 Hz, and the shear amplitude was 150%. To eliminate any residual stresses on the oriented microdomains during the shearing process, we annealed the oriented bulk samples for 12 h at 140 °C, which is above the glass transition temperature of P4VP blocks (T_g^{P4VP} = 130 °C) and well above the equilibrium melting temperature (T_m^0 = 69 °C) of PCL blocks. Consequently, the samples were subjected to further crystallization in DSC under a nitrogen atmosphere.

Differential Scanning Calorimeter (DSC). Nonisothermal and isothermal crystallization experiments of PCL blocks within the confined microdomain were examined using a differential scanning calorimeter (DSC-7 Perkin-Elmer) equipped with a mechanical intracooler. The DSC instrument was properly calibrated with an indium standard at a scan rate of 10 °C/min. Samples were annealed at 80 °C for 5 min and then rapidly cooled at 150 °C/min to preset temperatures for isothermal crystallization. After crystallization, the scan rate of 10 °C/min was employed to record the endotherms of the PCL crystals in the P4VP−PCL BCPs. For nonisothermal crystallization experiments, the crystallization peak temperature of the exotherms (T_f) of the samples were recorded by a cooling rate of −10 °C/min from the melt state at 80 °C.

Transmission Electron Microscopy (TEM). Prior to TEM characterization, the bulk P4VP−PCL samples were isothermally

---

*To whom the correspondence should be addressed: Tel 886-3-5738349, Fax 886-3-5715408, e-mail rmho@mx.nthu.edu.tw (R.-M.H.); Tel 886-3-4227151 ext 34205, Fax 886-3-4252296, e-mail yssun@cc.ncu.edu.tw (Y.-S.S.).

Table 1. Characterization of P4VP−PCL BCPs

sample[a]	M_n^{total} (kg/mol)	M_n^{P4VP} (kg/mol)[b]	M_n^{PCL} (kg/mol)[b]	M_w/M_n[c]	f_{PCL}[v]	d_{PCL}[d] (nm)
VP/CL 142/46	20.4	15.0	5.4	1.27	0.25	17.8
VP/CL 90/38	13.9	9.5	4.4	1.22	0.30	14.8
VP/CL 50/26	8.3	5.3	3.0	1.25	0.34	13.7
VP/CL 90/23	12.2	9.5	2.7	1.18	0.21	10.3
VP/CL 85/23	11.7	9.0	2.7	1.15	0.22	9.9

[a] VP/CL *m*/*n*, where *m* and *n* represent the degree of polymerization of the constituted P4VP (N_{P4VP}) and PCL (N_{PCL}) blocks, respectively. [b] M_n^{P4VP} and M_n^{PCL} were characterized by proton nuclear magnetic resonance (^{1}H NMR) and gel permeation chromatography (GPC). [c] Polydispersity index (PDI) of BCPs was determined by GPC using standard calibration. [d] The diameters of PCL cylinders (d_{PCL}) for the P4VP−PCL samples were calculated by combining the determined interdomain distances and the volume fractions of PCL blocks (f_{PCL}[v]). The cylindrical microdomains were determined by TEM and SAXS (cf. Figures S1 and S2). The cylindrical microdomains of the synthesized P4VP−PCL with various molecular weights were determined by SAXS.

melt-crystallized in DSC, and then extracted from DSC pans, followed by ultra-cryomicrotoming at −120 °C using a Reicher Ultracut microtome (equipped with a Reichert FCS cryo-chamber and a diamond knife). Staining was achieved by exposing the microtomed thin films to the vapors of a 4% aqueous RuO_4 solution for 30 min. A JEOL JEM-1200x transmission electron microscope was used (accelerating voltage: 120 keV).

Small-Angle X-ray Scattering (SAXS) and Wide-Angle X-ray Diffraction (WAXD). 2D SAXS/WAXD experiments were performed at the wiggler beamline BL17B3 at the National Synchrotron Radiation Research Center (NSRRC), Taiwan. The incident X-ray beam was focused vertically by a spherical mirror and monochromated to the energy of 12 keV by a Si(111) double-crystal monochromator (DCM). The wavelength of the X-ray beam was λ = 1.03 Å. The distance from sample to detector was 2749.7 mm, and the beam stop was a Tantalum disk 4 mm in diameter. SAXS data were collected using a two-dimensional gas-filled area detector, and the sensitivity of the 2D detector was calibrated by using a ^{55}Fe source before data collection. The calibration of the detector pixels in terms of scattering vector was made by linear regression over the positions of numerous orders of the long period of silver behenate as the standard, with q_{max} being 1.076 nm^{-1}; $q = (4\pi/\lambda)\sin(\theta/2)$, with scattering angle θ. The 2D WAXD patterns were collected on Fuji plates using X-rays from a synchrotron. 2D WAXD images were collected for 3 min for each data acquisition and were calibrated using α-Al_2O_3. A contribution from air scattering was subtracted from both 2D SAXS and WAXD patterns. Azimuthally integrated profiles were extracted from the 2D WAXD patterns for further analysis.

Results and Discussion

For crystallization temperatures (T_fs) with a maximum crystallization rate during cooling in nonisothermal crystallization experiments, as shown in Figure 1, we found variations in T_fs of PCL blocks for the cylinder-forming P4VP−PCL BCPs with different domain sizes (i.e., different confinement sizes). Particularly, VP/CL 90/23 (10.3 nm) and 85/23 (9.9 nm) reveal a significant shift in T_f to a low temperature out of the region −30 to 80 °C. This indicates that when the confined size is below 10 nm, the crystallization of PCL blocks becomes difficult. Therefore, the crystallization temperature for the confinement size below 10 nm is not easily discernible during the cooling process ranging from 80 to −30 °C in DSC.

We further examined the crystallization kinetics. The dependence of crystallization half-time ($t_{1/2}$) on the crystallization temperature (T_c) and d_{PCL} (i.e., the confined size) was examined. As shown in Figure 2, large undercooling is required to induce crystallization within the 10 nm size confined cylindrical microdomain. Namely, VP/CL 90/23 and 85/23 only crystallized at low temperatures below −45 °C. The upward shift of $t_{1/2}$ (T_c) upon decreasing d_{PCL} from 17.8 nm (VP/CL 142/46) to 13.7 nm (VP/CL 50/26) indicates a significant effect of confined size on the rate of crystallization. Moreover, for high crystallization temperatures, this effect becomes much more pronounced than that in the corresponding homopolymer having same molecular weight. Also, the $t_{1/2}$ (T_c) curve of PCL crystallization significantly shifts to a low temperature when the confined size is decreased to 10 nm. Generally, for crystallization at high temperatures, such as the temperature for crystallization close to the T_m^0 of PCL crystallites, favors the growth of thick PCL crystalline stems with less chain folding. We thus speculate that this significant shift in the $t_{1/2}$ curve is attributed to energetic barriers arising from the existence of effective confinement.

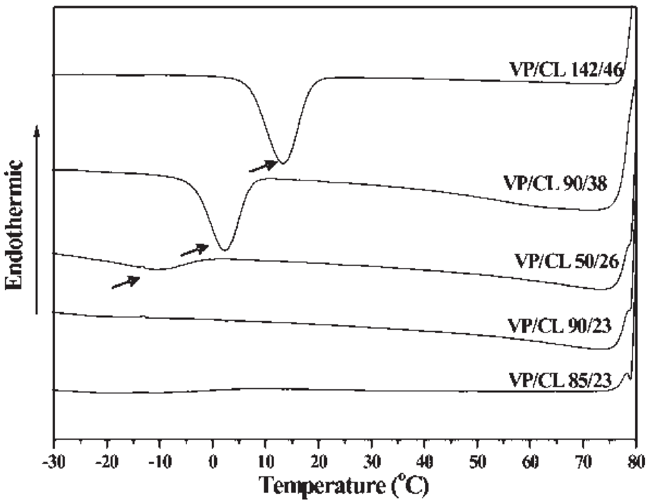

Figure 1. Nonisothermal crystallization exotherms of P4VP−PCL samples. The cooling rate was −10 °C/min.

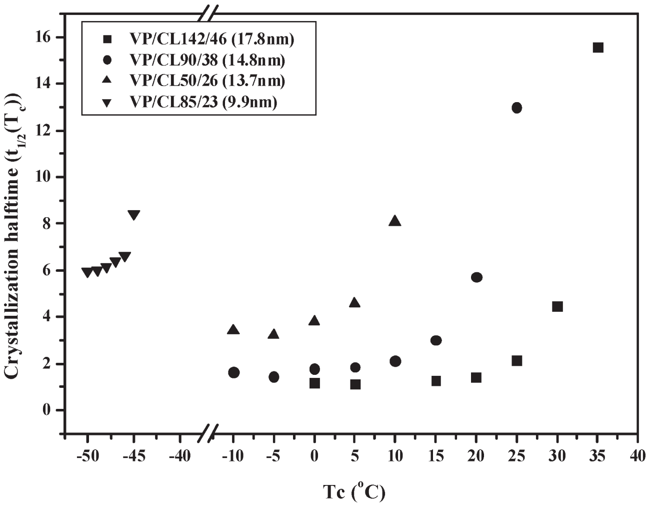

Figure 2. Dependence of crystallization half-time ($t_{1/2}$) of isothermal crystallization for P4VP−PCL BCPs with different confined sizes.

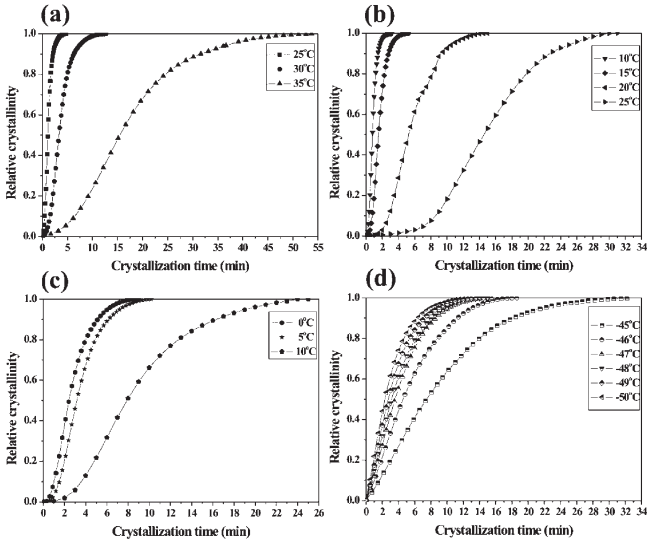

Figure 3. Development of crystallinity during isothermal crystallization at different T_cs in (a) VP/CL 142/46, (b) VP/CL 90/38, (c) VP/CL 50/26, and (d) VP/CL 85/23. The relative crystallinity was deduced from the change of enthalpy during dynamic isothermal crystallization in DSC.

The isothermal crystallization is satisfactorily described with the Avrami equation by $X_C(t) = 1 - \exp(-Kt^n)$ where $X_C(t)$ is the normalized degree of crystallinity that has formed at time t, and the prefactor K and exponent (index) n are Avrami parameters.[10] The dynamic process of isothermal crystallization under confinement was monitored by the change of enthalpy in DSC. From the DSC analyses of Avrami index (Figure 3), the curve of exothermic response with crystallization time exhibits a noticeable transition from low to high crystallization temperature. Also, the curve of exothermic response with the duration of crystallization exhibits a simple exponential shape prescribed by exponential-like crystallization kinetics for a 10 nm size confinement, suggesting a homogeneous nucleation (Figure 3d). By contrast, in the case of BCPs with a larger confined size, such as 17.8, 14.8, or 13.7 nm, the crystallization of the PCL blocks within cylindrical microdomain reveals that the exothermic curve exhibits sigmoidal crystallization kinetics for crystallization. The sigmoidal curves prescribed by Avrami index values greater than unity reflects a spreading growth habit by a long-range (typically micrometer range) growth of crystallites.[20]

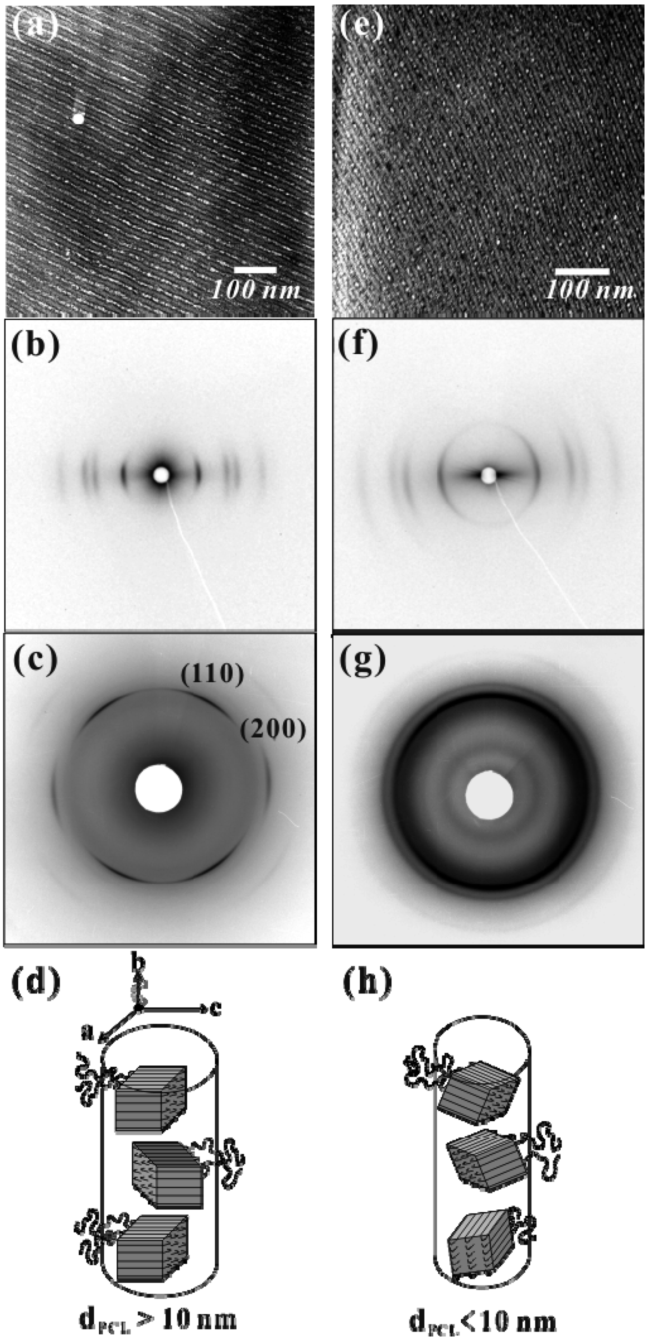

Figure 4. VP/CL 90/38 system: (a) TEM image (T_c = 10 °C), (b) 2D anisotropic SAXS pattern, (c) fiberlike WAXD pattern with incident X-ray beams along the gradient direction, and (d) the schematic illustration of crystalline chain orientation under confinement. VP/CL 85/23 system: (e) TEM image (T_c = −50 °C), (f) 2D anisotropic SAXS pattern, and (g) ringlike WAXD pattern with incident X-ray beams along the gradient direction and (h) the schematic illustration of crystalline chain orientation under confinement.

We further performed the TEM observation and simultaneous 2D SAXS/WAXD experiments to identify the morphological evolution while confined size is larger than 10 nm. A cylindrical microdomain orientation with respect to the shear geometry is defined in Figure S3. The crystal stems, generating via a heterogeneous nucleation, grow with time and finally spread over the scale of a few tens of micrometers (Figure 4a). By contrast, the side view of cylindrical microdomains displays discrete granules, reflecting that the granules yield via a homogeneous nucleation (Figure 4e). Crystallization within such discrete spherelike granules is analogous to the homogeneous nucleation of poly(ethylene oxide) (PEO) confined to spherical microdomains of highly asymmetric BCPs.[5,10,11,15,20] Moreover, as evidenced by X-ray results, the slablike crystallites of PCL originating from the heterogeneous nucleation have a perpendicular orientation where the *b*-axis of the PCL crystals is parallel to the cylindrical axis (Figure 4b,c). Granule-like crystallites that yield via the homogeneous nucleation within the cylindrical microdomains reveal a random orientation (Figure 4f,g). The WAXD reflections were indexed on the basis of an orthorhombic unit cell with dimensions $a = 0.7096$ nm, $b = 0.4974$ nm, and $c = 1.7297$ nm.[21] Referring to the orthorhombic lattice structure of PCL crystals, the observed reflections could be indexed as (110) and (200) reflections as shown in Figure 4c. The WAXD pattern of the 10 °C-crystallized VP/CL 90/38 displays a maximum diffraction intensity of (110) reflection locating at the azimuthal angles, $\Phi = 53°$, 125°, 231°, and 300°; the maximum diffraction intensity of (200) reflection is at $\Phi = 0$ and 180°. A comparison between the WAXD and its corresponding SAXS pattern suggests a perpendicular orientation of PCL crystallites for the VP/CL 90/38 sample crystallized at high temperatures; namely, the preferential growth of the *b*-axis of PCL crystallites (the fastest growth direction) follows the cylindrical axes. The preferred crystalline orientation is referred to the restriction of confined microdomain on the nucleation density and crystalline growth.[5,10−12] In the case of the large confined size (i.e., ∼14.7 nm), considering the kinetics of crystallization, the crystal growth direction might selectively follow an unrestricted pathway to reach a fast growth rate (Figure 4d). Also, considering the thermodynamics of crystallization, the crystallinity must reach a maximum within a short time period. At the stage, the polymer is expected to have a minimum Gibbs free energy upon achieving the maximum of crystallinity during the crystallization process.[22] Both considerations explain why the PCL crystal growth within the cylindrical microdomain of 14.7 nm appears as perpendicular orientation. When the confined space is reduced to be below a critical size (i.e., 10 nm), the crystal orientation alters from perpendicular orientation to random orientation (Figure 4h). The reason is that under such a confinement polymeric crystallization only occurs at low temperatures, at which homogeneous nucleation initiates to form a state with high density of nuclei. Since the subsequent crystal growth is limited by the constrain of both the space of cylindrical spatial confinement and the nuclei themselves, the primary nucleation dominates the overall crystallization process, resulting in tiny granules with a random orientation.[2k,17]

Conclusions

To conclude, for 2D confinement (i.e., cylindrical confinement) a specific crystalline orientation can be directed by the cylindrical confinement to kinetically achieve the fast path for crystalline growth. For the larger confined sizes, the crystalline chains of PCL appear as a perpendicular orientation with respect to the cylindrical axis having a preferred growth direction along the *b*-axis (i.e., the fastest crystalline growth direction of PCL crystallite) parallel to the cylinder axes. By contrast, as the confinement size further decreases to reach an effective confined size, at which size homogeneous nucleation governs the overall polymer crystallization since the nuclei yields at a high density at deep undercooling. As a result, small crystalline granules with random orientation yield within the confined space of cylindrical microdomains.

Acknowledgment. The authors thank the National Science Council of the Republic of China, Taiwan, for financially supporting this research under Contract NSC 97-2221-E-007-035-MY3. Dr. Lixia Rong and Prof. Benjamin Hsiao at beamline X27C at National Synchrotron Light Source and Drs. Ying-Hung Lai and U-Ser Jeng at beamline BL17B3 at National Synchrotron Radiation Research Center, Taiwan, are appreciated for their help in SAXS and WAXD experiments, respectively.

Supporting Information Available: Figures showing TEM and SAXS characterizations of cylindrical microdomains, and the microdomain orientation in a shear field. This material is available free of charge via the Internet at http://pubs.acs.org.

References and Notes

(1) (a) Wang, H.; Keum, J. K.; Hiltner, A.; Baer, E.; Freeman, B.; Rozanski, A.; Galeski, A. *Science* **2009**, *323*, 757–760. (b) Zhang, Q.; Wang, M.; Wooley, K. L. *Curr. Org. Chem.* **2005**, *9*, 1053.

(2) (a) Nojima, S.; Kato, K.; Yamamoto, S.; Ashida, T. *Macromolecules* **1992**, *25*, 2237–2242. (b) Rangarajan, P.; Register, R. A.; Fetters, L. J.; Bras, W.; Naylor, S.; Ryan, A. J. *Macromolecules* **1995**, *28*, 4932–4938. (c) Rangarajan, P.; Register, R. A.; Fetters, L. J. *Macromolecules* **1993**, *26*, 4640–4645. (d) Ryan, A. J.; Hamley, I. W.; Bras, W.; Bates, F. S. *Macromolecules* **1995**, *28*, 3860–3868. (e) Cohen, R. E.; Cheng, P. L.; Douzinas, K.; Kofinas, P.; Berney, C. V. *Macromolecules* **1990**, *23*, 324–327. (f) Douzinas, K. C.; Cohen, R. E. *Macromolecules* **1992**, *25*, 5030–5035. (g) Cohen, R. E.; Bellare, A.; Drzewinski, M. A. *Macromolecules* **1994**, *27*, 2321–2323. (h) Hamley, I. W.; Fairclough, J. P. A.; Terrill, N. J.; Ryan, A. J.; Lipic, P. M.; Bates, F. S.; Towns-Andrews, E. *Macromolecules* **1996**, *29*, 8835–8843. (i) Quiram, D. J.; Register, R. A.; Marchand, G. R.; Adamson, D. H. *Macromolecules* **1998**, *31*, 4891–4898. (j) Zhu, L.; Cheng, S. Z.-D.; Calhoun, B. H.; Ge, Q.; Quirk, R. P.; Thomas, E. L.; Hsiao, B. S.; Yeh, F.; Lotz, B. *Polymer* **2001**, *42*, 5829–5839. (k) Zhu, L.; Calhoun, B. H.; Ge, Q.; Quirk, R. P.; Cheng, S. Z.-D.; Thomas, E. L.; Hsiao, B. S.; Yeh, F.; Liu, L.; Lotz, B. *Macromolecules* **2001**, *34*, 1244–1251. (l) Kofinas, P.; Cohen, R. E. *Macromolecules* **1994**, *27*, 3002–3008. (m) Quiram, D. J.; Register, R. A.; Marchand, G. R. *Macromolecules* **1997**, *30*, 4551–4558. (n) Mai, S.-M.; Fairclough, J. P. A.; Viras, K.; Gorry, P. A.; Hamley, I. W.; Ryan, A. J.; Booth, C. *Macromolecules* **1997**, *30*, 8392–8400.

(3) Zhu, L.; Cheng, S. Z. D.; Calhoun, B. H.; Ge, G.; Quirk, R. P.; Thomas, E. L.; Hsiao, B. S.; Yeh, F.; Lotz, B. *J. Am. Chem. Soc.* **2000**, *122*, 5957–5967.

(4) Loo, Y. L.; Register, R. A.; Ryan, A. J. *Phys. Rev. Lett.* **2000**, *84*, 4120–4123.

(5) Hobbs, J. K.; Register, R. *Macromolecules* **2006**, *39*, 703–710.

(6) Huang, P.; Zhu, L.; Guo, Y.; Ge, Q.; Jing, A. J.; Chen, W. Y.; Quirk, R. P.; Cheng, S. Z. D.; Thomas, E. L.; Lotz, B.; Hsiao, B. S.; Avila-Orta, C. A.; Sics, I. *Macromolecules* **2004**, *37*, 3689–3698.

(7) Chen, H. L.; Hsiao, S. C.; Lin, T. L.; Yamauchi, K.; Hasegawa, H.; Hashimoto, T. *Macromolecules* **2001**, *34*, 671–674.

(8) Chen, H.-L.; Wu, J. C.; Lin, T.-L.; Lin, J. S. *Macromolecules* **2001**, *34*, 6936–6944.

(9) Loo, Y.-L.; Register, R. A.; Ryan, A. J.; Dee, G. T. *Macromolecules* **2001**, *34*, 8968–8977.

(10) Loo, Y.-L.; Register, R. A.; Ryan, A. J. *Macromolecules* **2002**, *35*, 2365–2374.

(11) Woo, E.; Huh, J.; Jeong, Y. G.; Shin, K. *Phys. Rev. Lett.* **2007**, *98*, 136103.

(12) Shin, K.; Woo, E.; Jeong, Y. G.; Kim, C.; Huh, J.; Kim, K.-W. *Macromolecules* **2007**, *40*, 6617–6623.

(13) (a) De Rosa, C.; Park, C.; Thomas, E. L.; Lotz, B. *Nature* **2000**, *405*, 433–437. (b) Park, C.; De Rosa, C.; Thomas, E. L. *Macromolecules* **2001**, *34*, 2602–2606.

(14) (a) Reiter, G.; Gastelein, G.; Hoerner, P.; Riess, G.; Blumen, A.; Sommer, J.-U. *Phys. Rev. Lett.* **1999**, *83*, 3844–3847. (b) Reiter, G.; Castelein, G.; Sommer, J. U.; Röttele, A.; Thurn-Albrecht, T. *Phys. Rev. Lett.* **2001**, *87*, 226101-1–226101-4.

(15) (a) Massa, M. V.; Dalnoki-Veress, K. *Phys. Rev. Lett.* **2004**, *92*, 255509. (b) Massa, M. V.; Carvalho, J. L.; Dalnoki-Veress, K. *Phys. Rev. Lett.* **2006**, *97*, 247802−1–247802−4.

(16) (a) Steinhart, M.; Senz, S.; Wehrspohn, R. B.; Gösele, U.; Wendorff, J. H. *Macromolecules* **2003**, *36*, 3646–3651. (b) Steinhart, M.; Goring, P.; Dernaika, H.; Prabhukaran, M.; Gösele, U.; Hempel, E.; Thurn-Albrecht, T. *Phys. Rev. Lett.* **2006**, *97*, 027801.

(17) Sun, Y.-S.; Chung, T.-M.; Li, Y.-J.; Ho, R.-M.; Ko, B.-T.; Jeng, U.-S.; Lotz, B. *Macromolecules* **2006**, *39*, 5782–5788.

(18) Sun, Y.-S.; Chung, T.-M.; Li, Y.-J.; Ho, R.-M.; Ko, B.-T.; Jeng, U.-S. *Macromolecules* **2007**, *40*, 6778–6781.

(19) (a) Ko, B. T.; Lin, C. C. *Macromolecules* **1999**, *32*, 8296–8300. (b) Xia, J.; Zhang, X.; Matyjaszewski, K. *Macromolecules* **1999**, *32*, 3531–3533.

(20) (a) Müller, A. J.; Albuerne, J.; Marquez, L.; Raquez, J. M.; Degée, P.; Dubois, P.; Hobbs, J.; Hamley, I. W. *Faraday Discuss.* **2005**, *128*, 231–252. (b) Müller, A. J.; Albuerne, J.; Esteves, L. M.; Marquez, L.; Raquez, J. M.; Degée, P.; Dubois, P.; Collins, S.; Hamley, I. W. *Macromol. Symp.* **2004**, *215*, 369–382. (c) Müller, A. J.; Balsamo, V. M.; Arnal, L.; Jakob, T.; Schmalz, H.; Abetz, V. *Macromolecules* **2002**, *35*, 3048–3058.

(21) (a) Hu, H.; Dorset, D. L. *Macromolecules* **1990**, *23*, 4604–4607. (b) Bittiger, H.; Marchessault, R. H. *Acta Crystallogr.* **1970**, *B26*, 1923–1927.

(22) Chiang, Y.-W.; Ho, R.-M.; Thomas, E.-L.; Burger, C.; Hsiao, B.-S. *Adv. Funct. Mater.* **2009**, *19*, 448–459.